



Development of *in situ* NiAl–Al₂O₃ nanocomposite by reactive milling and spark plasma sintering

V. Udhayabanu^{a,b}, K.R. Ravi^{a,c}, B.S. Murty^{a,*}

^a Department of Metallurgical and Materials Engineering, Indian Institute of Technology Madras, Chennai 600 036, India

^b Department of Metallurgical Engineering, PSG college of Technology, Coimbatore, India

^c PSG Institute of Advanced Studies, Coimbatore, India

ARTICLE INFO

Article history:

Received 29 August 2010

Received in revised form 8 December 2010

Accepted 14 December 2010

Available online 22 December 2010

Keywords:

Nanostructured materials

Mechanical alloying

Solid state reaction

Transmission electron microscopy

Spark plasma sintering

ABSTRACT

NiAl–10 vol.% Al₂O₃ *in situ* nanocomposite has been synthesized by reactive milling and subsequent spark plasma sintering. The synthesized nanocomposites have ~96% of theoretical density after sintering at 1000 °C for 5 min. Microstructural analysis of consolidated samples using TEM has revealed the presence of α-Al₂O₃ particles of 10–12 nm size in NiAl matrix of submicron grain size. Consolidated NiAl–10 vol.% Al₂O₃ nanocomposite has shown very high hardness of 772 HV_{0.3} and compressive strength of 2456 MPa with ~14% plastic strain. The high hardness and compressive yield strength are attributed to the presence of nanocrystalline α-Al₂O₃ particles and the appreciable plastic strain is attributed to the submicron grains of NiAl.

© 2010 Elsevier B.V. All rights reserved.

1. Introduction

Ordered NiAl has relatively low density, high strength, high melting point, high thermal conductivity, excellent oxidation resistance. Due to these attractive properties ordered NiAl is considered as a potential candidate for high temperature parts of gas turbine engines for aircraft-propulsion systems, bond coats under thermal barrier coatings, electronic metallization compounds in advanced semiconductor heterostructures and surface catalysts. However, inadequate room temperature ductility is the limiting factor for this material to be used in structural applications [1–3]. Also, the structural use of ordered NiAl suffers from low toughness at ambient temperature and low strength and creep resistance at elevated temperatures. Among the possible methods to improve these properties, refining the microstructure and incorporating second phase particles are having the attention from various research groups since the ductility can be improved by the refined microstructure [4] and the creep resistance can be enhanced by the reinforced particulates [5].

The mechanical properties of NiAl can be improved by reinforcing them with particles such as Al₂O₃, TiB₂, TiC [6–9]. Development of *in situ* reinforcement is preferred because of the clean interface, thermodynamic stability and the uniform distribution [10].

Recently reactive milling has been used to synthesize *in situ* composites by activating the thermite reactions using high energy ball milling [11–13]. During reactive milling both matrix and reinforcement are formed through *in situ* process, which will promote good bonding between matrix and reinforcement. Moreover, a homogeneous distribution of fine reinforcing particles can be obtained by the Mechanical Alloying (MA) process [6,14]. The advantage in using reactive milling over other techniques is the establishment of nanocrystalline matrix as well as the reinforcements [15].

NiAl–TiC nanocomposite has been synthesized successfully by carrying out reactive milling of Ni, Al, Ti, and C powders [16,17]. The Al₂O₃ also has been proven to be a suitable reinforcement since it has low density, high specific strength, high modulus, and good oxidation resistance. Moreover its coefficient of expansion closely matches to NiAl matrix [3]. Development of NiAl–Al₂O₃ nanocomposites by mechanical alloying has been achieved by the milling of NiAl–Al₂O₃ [18], Ni₂(OH)₂CO₃·3H₂O–Al [19], Ni–Al–Al₂O₃ [20], and NiO–Al [21,22] powder mixture.

Recently, NiAl–Al₂O₃ composite has been developed by Anvari et al. [22] using reactive milling of NiO, Al and Ni powders without process controlling agent. Anvari et al. [22] have reported that the average crystallite size of α-Al₂O₃ formed after the combustive reaction in 0.5 h milling is 60 nm and further milling up to 60 h was needed to reduce the average crystallite size to 15 nm. The present authors [23] have developed NiAl–30 vol.% Al₂O₃ nanocomposites by reactive milling of NiO, Al and Ni powders in toluene medium and reported amorphous Al₂O₃ and NiAl with crystallite size of

* Corresponding author. Tel.: +91 044 22574754; fax: +91 044 22570509.
E-mail address: murty@iitm.ac.in (B.S. Murty).

7 nm after 20 h milling. After heating the as milled powder to 1120 °C the authors have observed α -Al₂O₃ particles of 11 nm distributed in NiAl matrix of 110 nm size. Presence of such fine α -Al₂O₃ would improve the hardness and yield strength of NiAl. This has been shown in the study of Oleszak [21] who has synthesized NiAl–42 vol.% Al₂O₃ nanocomposites by reactive milling of NiO, Al and Ni powders. However, the higher Al₂O₃ percentage in NiAl matrix may reduce the ductility. Hence, NiAl based nanocomposites with smaller amount of very fine Al₂O₃ particles may realize the combination of higher yield strength with good ductility.

The consolidation of nanocrystalline NiAl powders has been accomplished by different techniques like hot pressing [21,24,25], shock wave compaction [7], explosive compaction [21] and spark plasma sintering [26,27]. Among these consolidation techniques spark plasma sintering (SPS) has advantages of short sintering time and low sintering temperature [28]. It is probable to realize fine NiAl–Al₂O₃ nanocomposite with improved mechanical properties by combining reactive milling and spark plasma sintering.

The present study aims to develop *in situ* NiAl–10 vol.% Al₂O₃ nanocomposite using reactive milling followed by spark plasma sintering. The phase formation during reactive milling has been analyzed using XRD. The microstructure of consolidated samples has been studied using TEM. The mechanical properties like hardness, compressive strength and plastic strain have also been investigated.

2. Experimental details

Reactive milling was carried out for NiO (Alfa Aesar, 99% purity, –325 mesh) Al (Loba Chemie Pvt Ltd., 99.7% purity, –325 mesh) and Ni (Loba Chemie Pvt. 99.5% purity, –200 mesh) powders at a composition of NiO–33 wt.% Al–52.7 wt.% Ni using a planetary ball mill (Fritsch pulverisette-5) in order to get NiAl–10 vol.% Al₂O₃ nanocomposite powder. Milling was carried out at the ball to powder ratio of 10:1 using tungsten carbide vials and tungsten carbide balls of 10 mm diameter. Toluene was used as process controlling agent to avoid oxidation and excessive cold welding of powders to vials and balls. The milling speed was maintained as 300 rpm. Phase and structural evolution during milling and heating were analyzed using Bruker AXS X-ray diffractometer, with Cu K α radiation. Crystallite size calculation was made using Voigt X-ray peak profile analysis after eliminating the strain and instrumental broadening contributions [29]. Chemical analysis for Tungsten was carried out using Optima 5300 DV ICP-OES (Inductively Coupled Plasma-Optical Emission Spectroscopy) in order to find out the WC contamination in the 20 h milled powder. The as milled powders were consolidated to 5 mm \times 15 mm pellets in a graphite die and consolidated under a uniaxial pressure of 75 MPa, using a SPS-1050 apparatus (Sumitomo Metals, Japan) at 1000 °C for 5 min. Density of bulk samples was measured by Archimedes method.

Microstructural analysis was carried out for bulk consolidated samples using Philips CM20 transmission electron microscope (TEM) operating at 200 kV. For the TEM analysis, the samples were prepared by Ar-ion milling preceded by dimpling. The hardness of the compacts was measured using microhardness tester under a load of 300 g for 15 s. The average of 20 indentations was considered as the Vickers microhardness value. Compression test was carried out on 2.5 mm \times 3 mm cylindrical sample at the strain rate of 10^{–4} s^{–1}.

3. Results

Fig. 1 shows the XRD pattern for the reactant powder mixture corresponding to the nominal composition of NiAl–10 vol.% Al₂O₃ as a function of milling time. After 5 h milling, the NiO and Al peak intensities decrease, indicating that the reduction of NiO has been initiated. The extent of reaction with milling time is calculated approximately from the change in the integrated intensity of NiO using the expression mentioned elsewhere [23,30]. Since the most intense peak of NiO(200) is overlapping with NiAl(110) peak from 5 h milling, the extent of reduction was calculated using NiO(111) peak. Fig. 2 presents the percentage reduction of NiO with respect to milling time and the crystallite size of NiO. After 5 h of milling, the extent of reduction is calculated to be 13%. The formation of ordered NiAl phase is also noticed after 5 h of milling from the appearance of superlattice peaks of NiAl. After 10 h of milling, the Al peaks disappear and 45% of the reduction of NiO has been observed. The

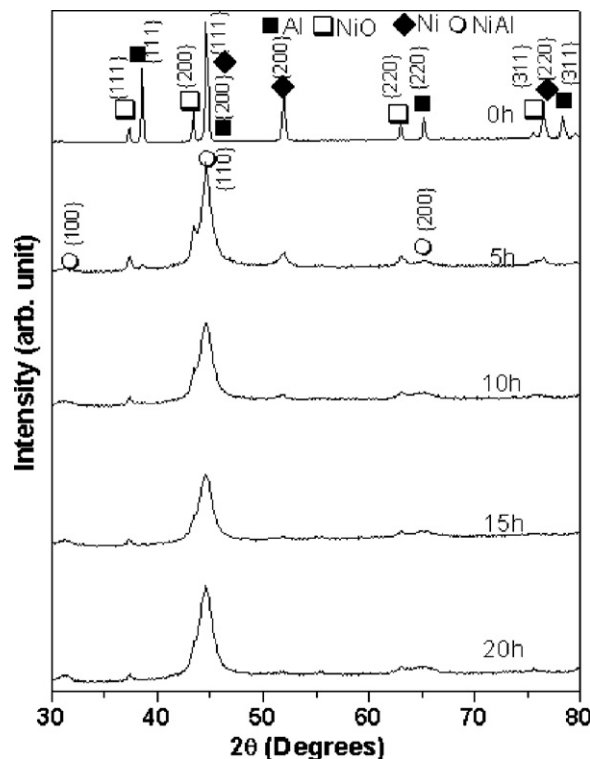


Fig. 1. XRD patterns of NiO–Al–Ni powder mixture corresponding to NiAl–10 vol.% Al₂O₃ as a function of milling time.

absence of the Al peaks after 10 h of milling indicates that the Al is consumed for the reduction of NiO as well as for the formation of the NiAl phase. As the milling progresses, reduction of NiO is more likely to be carried out by NiAl and the extent of reduction is increased to 65% after 20 h of milling leaving behind some amount of unreacted NiO. The absence of Al₂O₃ peaks in 20 h milled is possibly due to the amorphous nature and its smaller quantity [30]. ICP-OES results has shown ~0.2 wt.% of W contamination in 20 h milled powder.

The calculated crystallite size and lattice strain of *in situ* formed NiAl phase with respect to milling time is shown in Fig. 3. The calculated crystallite size of the NiAl phase after 5 h of milling is 19 nm and after 15 h milling it is reduced to 13 nm and it remains same till

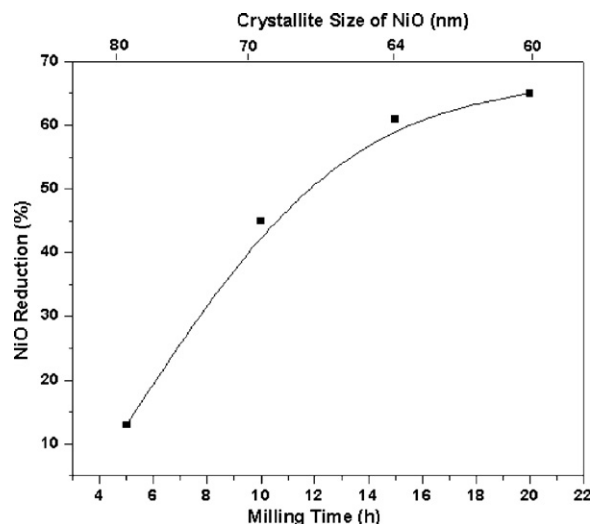


Fig. 2. Percentage reduction of NiO as a function of milling time and crystallite size of NiO.

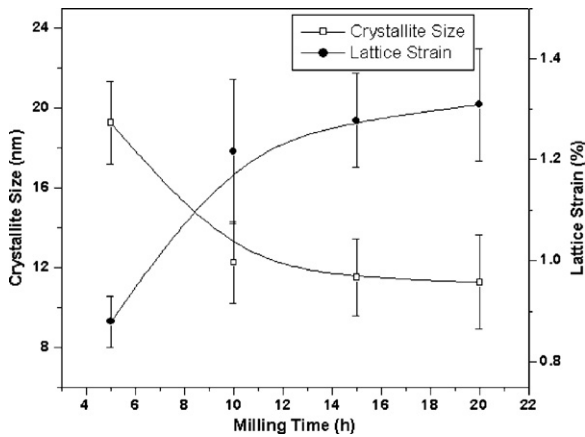


Fig. 3. Crystallite size and lattice strain of NiAl as a function of milling time.

20 h milling. The calculated lattice strain after 5 h milling is 0.89% and it increases to 1.18% after 20 h milling.

The long range order parameter, S , of the NiAl phase is calculated in the following way

$$S = \left[\frac{(I_{100}/I_{110})_{\text{obs}}}{(I_{100}/I_{110})_{\text{std}}} \right]^{0.5} \quad (1)$$

where the subscripts (obs) and (std) correspond to the intensity ratio of the superlattice reflection and the fundamental reflection in the XRD pattern of the sample and standard JCPDS file, respectively. NiAl phase formed is partially ordered and after 20 h of milling the order parameter (S) is measured to be 0.5. Disorder of B2 compounds by mechanical alloying is a common phenomenon and the disordering is due to the creation of point defects and the dislocations during milling [31]. The degree of order during milling is the balance between the disordering due to the defects created by mechanical alloying and the thermally activated reordering. Since the NiAl has the low enthalpy of formation, it has more tendency to reorder according to the Bragg–Williams theory [7]. Hence, the NiAl formed is not completely disordered.

The as milled powder was consolidated using SPS at 1000 °C. Fig. 4 shows the XRD pattern of NiAl–10 vol.% Al₂O₃ nanocomposite after the consolidation. The XRD pattern shows the presence of α -Al₂O₃ phase along with NiAl phase in the consolidated sample. The order parameter calculation has shown that the order parameter is increased from 0.5 in as milled powder to 0.7 in 1000 °C

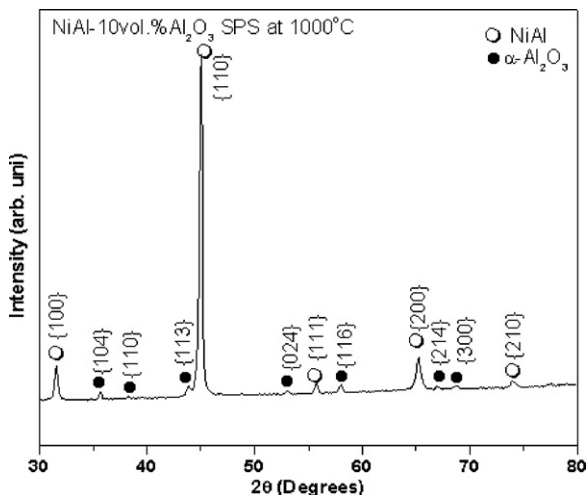


Fig. 4. XRD pattern of NiAl–10 vol.% Al₂O₃ after the consolidation by SPS.

SPS sample. The observed increase in degree of ordering after the SPS consolidation is attributed to the annealing of defects created during ball milling [31].

The TEM micrographs of NiAl–10 vol.% Al₂O₃ sintered at 1000 °C are shown in Fig. 5. The corresponding SAD spotty ring pattern consists of diffraction rings from NiAl, α -Al₂O₃ and Al₄C₃ phases (Fig. 5(b)). The presence of Al₄C₃ particles is possibly due to the carbon pick up from toluene medium. The grain size of NiAl measured from the dark field image obtained from NiAl(1 1 1) diffraction plane is 227 ± 108 nm (Fig. 5(c) and (d)). The dark field image of α -Al₂O₃ obtained at low and higher magnifications are presented in Fig. 5(e) and 5(f), respectively. Fig. 5(e) shows the distribution of α -Al₂O₃ particles in NiAl matrix. Fig. 5(f) shows that the size of α -Al₂O₃ particle is 10–12 nm.

Since the XRD and TEM analysis of the compacted samples show that the reaction is complete the theoretical density of the synthesized nanocomposites is calculated using rule of mixture based on the aimed amount of phases. The density of NiAl–10 vol.% Al₂O₃ nanocomposite is measured to be 96% of theoretical density. The measured hardness of the synthesized NiAl–10 vol.% Al₂O₃ nanocomposite after the consolidation is 772 HV_{0.3}. The compression test result of NiAl consolidated at 1000 °C is presented in Fig. 6. The NiAl–10 vol.% Al₂O₃ nanocomposite has shown high yield strength of 2456 MPa with plastic strain of ~14%.

4. Discussion

4.1. Phase formations in NiAl–Al₂O₃ nanocomposite

In the present study, the TEM analysis of NiAl–10 vol.% Al₂O₃ nanocomposite has shown that the α -Al₂O₃ particles are in 10–12 nm size even after the consolidation at 1000 °C. On the other hand, Anvari et al. [22] have reported that the average crystallite size of α -Al₂O₃ formed after the combusive reaction in 0.5 h milling is 60 nm and further milling up to 60 h was needed to reduce the average crystallite size to 15 nm. However, there is a possibility of increase in the crystallite size of α -Al₂O₃ during consolidation of powders as the literature has shown that the consolidation of NiAl and NiAl based composites require above 1000 °C [7,21,24–27]. The major difference between the present study and the study by Anvari et al. [22] is the milling condition. Anvari et al. [22] have carried out dry milling for NiO–Al–Ni powder whereas in the present work, the milling has been carried out in the toluene medium (wet milling). In toluene medium, the reduction of NiO by Al and NiAl phase formation occur simultaneously and the reactions progress gradually despite of its high exothermicity as the toluene adhered on the surface reduces the activities of the reactant particles and the reaction rate [30]. Hence, the Al₂O₃ formed in the as milled condition might be in amorphous and during consolidation it transforms to fine and stable α -Al₂O₃ via the formation of γ -Al₂O₃ [30]. The reduction of NiO by Al is reported to be combusive during dry milling by other researchers since the adiabatic temperature for this reaction exceeds 3500 °C according to the thermodynamic calculations [7,21,22]. Since Anvari et al. [22] have performed the milling without process controlling agent, the local heat rise due to the exothermic displacement reaction possibly has resulted slightly coarser and crystalline α -Al₂O₃ during milling instead of amorphous or transition alumina.

4.2. Analysis on mechanical properties of NiAl–Al₂O₃ nanocomposite

Fig. 7 compares previously published mechanical properties of NiAl to that observed in the present work under the compression mode for NiAl–Al₂O₃ nanocomposite. The values of yield strength

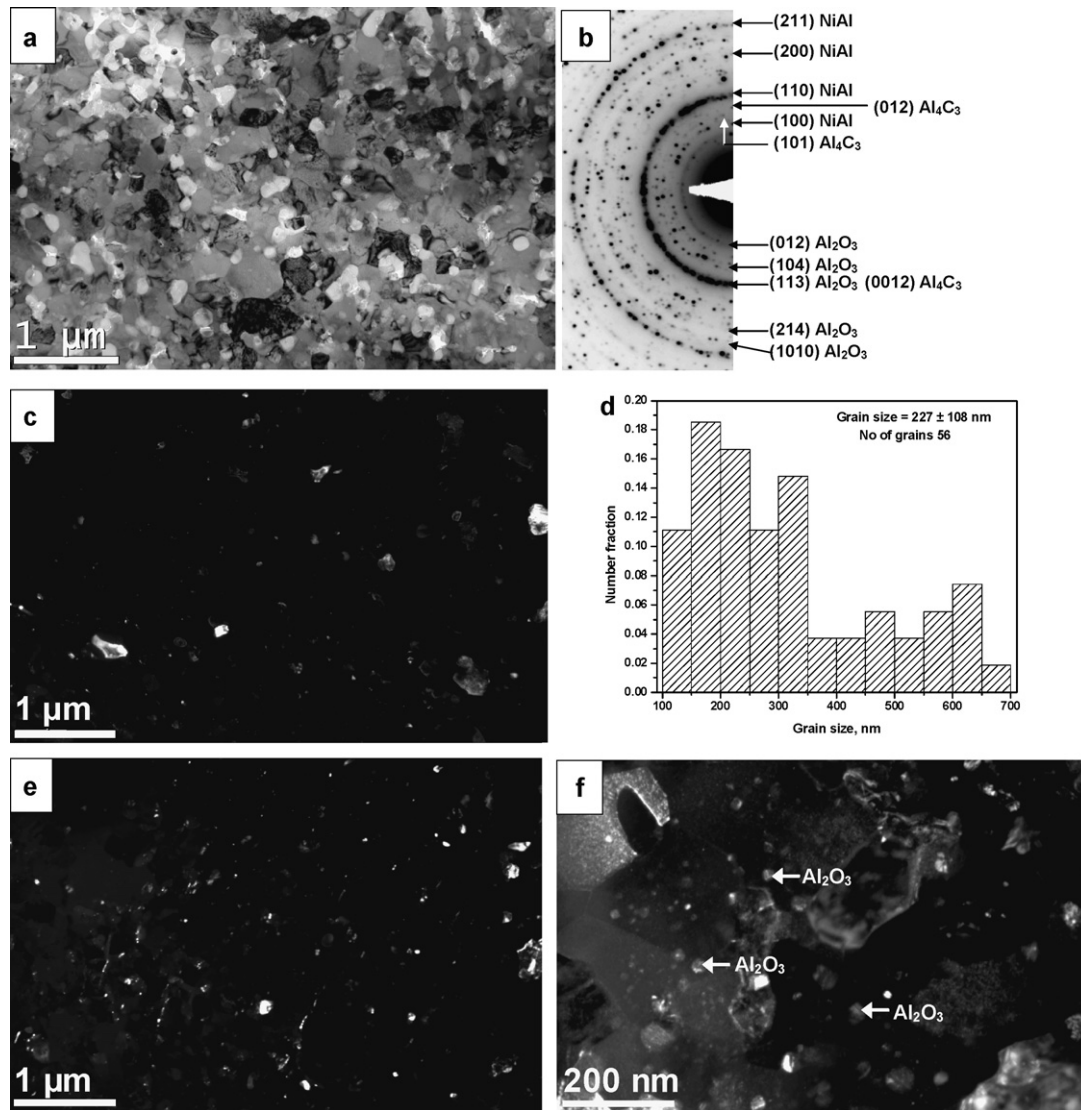


Fig. 5. TEM micrographs of NiAl–10 vol.% Al₂O₃ SPS at 1000 °C (a) bright field image, (b) SAD pattern, (c) dark field image obtained from NiAl(110) plane, (d) grain size distribution plot of NiAl matrix, (e) dark field image obtained from Al₂O₃(012) plane at low magnification. (f) dark field image obtained from Al₂O₃ at high magnification.

have been taken from these reports and plotted as a function of plastic strain to failure. To assist interpretation, these literature data are classified into four groups, representing (i) microcrystalline, (ii) submicron or ultrafine grain, (iii) nanocrystalline and (iv) bimodal grain structured NiAl.

In general, higher strength is achieved with the loss of plasticity. However, it has not been observed in the microcrystalline NiAl data, since this data involves addition of appreciable amount of alloying elements to improve the mechanical properties. For example, NiAl prepared by Guo et al. [32], Du et al. [33], Chen et al. [34,35] contains 28%Cr–5%Mo, 8%Cr–3.5%Nb, 7–14%Co and 2%Cr–0.2%Ce, respectively. These alloying elements form intermetallic compounds in NiAl matrix and the strength and ductility of these alloys not only depend on the grain size of NiAl but also on the type, size and morphology of intermetallic compounds of the added alloying elements. Moreover, the processing routes for the preparation of NiAl are vastly different (conventional ingot casting, injection casting, hot pressing and exothermic dispersion, suction casting). Hence, there may not be a particular trend observed between strength and ductility in microcrystalline data reported in the literature.

Kim et al. [27] have reported 1400 MPa compressive yield strength for NiAl with 80 nm grain size, synthesized by MA and SPS

at 1100 °C. However, nil ductility was observed. The reason for the low plastic strain is the lack of dislocation activity, lowering strain-hardening capability which leads to the shear band deformation mechanism observed in the nanocrystalline microstructure. Albitzer

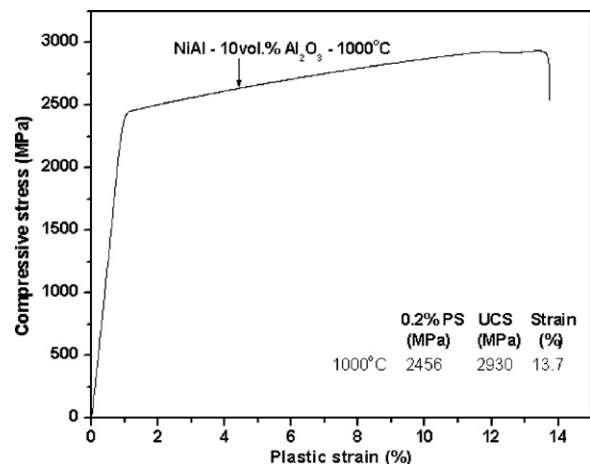


Fig. 6. Compressive stress–strain curve of NiAl–10 vol.% Al₂O₃.

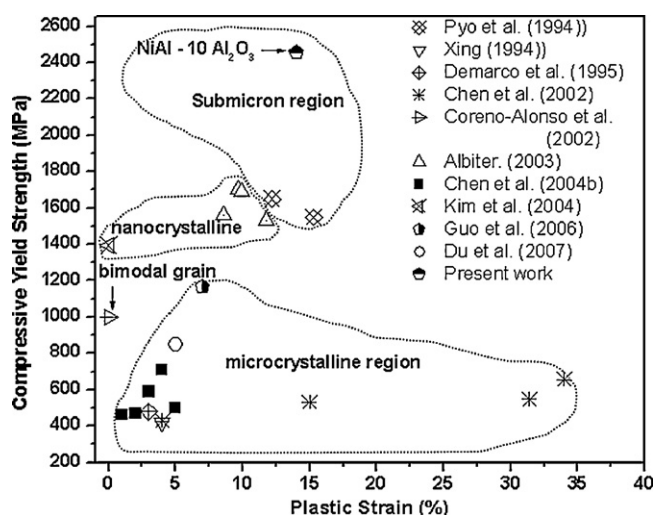


Fig. 7. A comparison of compressive mechanical properties of NiAl from previous reports with those in the current work.

et al. [25] have shown strain of 9–11% in NiAl of ~ 23 nm crystallite size, prepared by mechanical milling and hot pressing at 1200°C for 30 min and 1500°C for 15 min. The literature shows that TEM analysis of NiAl sintered at 1000°C or above has submicron range grain size [24,36,37]. The crystallite size of NiAl reported by Albiter et al. [25] after the consolidation was measured by Scherrer's formula using X-ray peak broadening. Moreover, Albiter et al. [25] have not reported the TEM analysis of hot pressed samples to support the results obtained in the XRD. Interestingly, the mechanical property results reported by Albiter et al. [25] fall close to the range of mechanical properties of submicron NiAl reported by Pyo et al. [24]. It further substantiates that the crystallite size reported by Albiter et al. [25] is possibly in the submicron range.

Coreno-Alonso et al. [26] have reported 1000 MPa compressive yield strength with nil ductility for NiAl with bimodal grain structure (10–30 nm and 0.5–2 μm), which has been synthesized by MA and SPS at 1000°C . The yield strength value calculated from hardness value reported by Coreno-Alonso et al. [26] is 800 MPa higher than the compressive yield strength value reported by them. It indicates that the brittle nature of the sample possibly made it fracture before the yielding. According to the literature, bimodal grain structure would result high strength with good ductility [38–40]. However, the reason for the nil ductility observed by the Coreno-Alonso et al. [26] in NiAl with bimodal grain structure is not understood.

It has been inferred from the collected mechanical properties data that the nanocrystalline NiAl would result very high yield strength with very low ductility and submicron grain structured NiAl has slightly lower yield strength with appreciable amount of plastic strain. The yield strength values obtained in the present work for NiAl–10 vol.% Al_2O_3 nanocomposites with submicron grain size are much higher than that of both submicron and nanocrystalline NiAl reported in the literature. Plastic strain observed in the present work is similar for the NiAl with submicron grain structure. The possible explanation for the observed high strength with improved ductility in the present work has been discussed in the following section.

The microstructure of NiAl–10 vol.% Al_2O_3 nanocomposite prepared in the present study consists of submicron NiAl grains together with $\alpha\text{-Al}_2\text{O}_3$ particles. Fig. 8 shows the hardness and grain size data in a Hall–Petch form for the NiAl–10 vol.% Al_2O_3 nanocomposite, together with data from several reports for NiAl [7,24,27,41,18] and NiAl– Al_2O_3 [21]. Due to the presence of large amount of Al_2O_3 particles, the hardness value of NiAl–42.5 vol.%

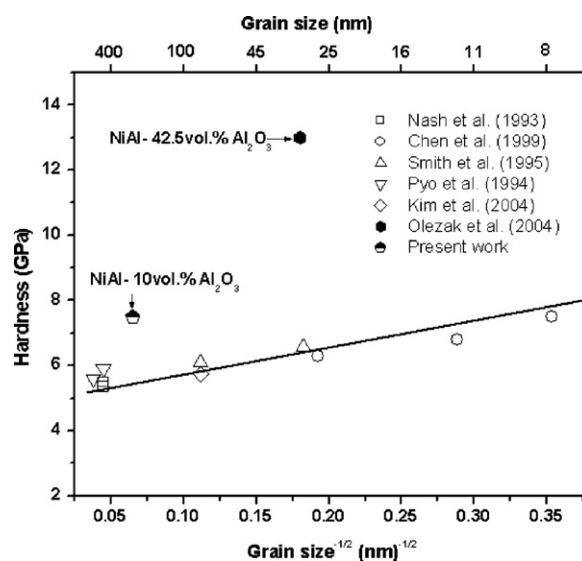


Fig. 8. Hall–Petch plot for NiAl and NiAl based nanocomposites.

Al_2O_3 nanocomposites synthesized by Oleszak [21] 6.5 GPa higher than that of NiAl with similar grain size. In the present work, the measured hardness of NiAl–10 vol.% Al_2O_3 nanocomposite is 7.6 GPa, which is 2.0 GPa higher than the literature data for NiAl with similar grain sizes (lying on the Hall–Petch line). This result suggests that the presence of $\alpha\text{-Al}_2\text{O}_3$ particles of 10–12 nm size is responsible for the improved hardness and yield strength.

5. Conclusions

NiAl based *in situ* nanocomposite reinforced with 10 vol.% Al_2O_3 has been developed successfully by reactive milling of NiO–Al–Ni powder mixture in toluene medium followed by the consolidation using SPS. Gradual NiO reduction by Al and simultaneous NiAl formation have been observed during milling. Microstructure of consolidated nanocomposite consists of $\alpha\text{-Al}_2\text{O}_3$ particles of 10–12 nm size and NiAl matrix with submicron grain size. The developed NiAl–10 vol.% Al_2O_3 nanocomposite exhibits very high hardness of 772 $\text{HV}_{0.05}$ and compressive strength of 2456 MPa with $\sim 14\%$ plastic strain. The higher hardness and compressive yield strength are attributed to the presence of $\alpha\text{-Al}_2\text{O}_3$ particles of 10–12 nm size and the appreciable plastic strain is due to the submicron grains of NiAl.

References

- [1] D.B. Miracle, *Acta Metall. Mater.* 41 (1993) 649–684.
- [2] S. Dymek, M. Dollar, S.J. Hwang, P. Nash, *Mater. Sci. Eng.* 152A (1992) 160–165.
- [3] M. Khodaei, M.H. Enayati, F. Karimzadeh, *J. Mater. Sci.* 43 (2008) 132–138.
- [4] H. Gleiter, *Prog. Mater. Sci.* 33 (1989) 223–315.
- [5] L. Wang, N. Beck, R. Arsenaut, *J. Mater. Sci. Eng.* 177A (1994) 83.
- [6] C.C. Koch, *Mater. Sci. Eng.* 244A (1998) 39–48.
- [7] T. Chen, J.M. Hampikian, N.N. Thadhani, *Acta Mater.* 47 (1999) 2567–2579.
- [8] H.X. Zhu, R. Abbaschian, *Mater. Sci. Eng.* 282A (2000) 1–7.
- [9] A. Milchalski, J. Jaroszewicz, M. Rosinski, D. Sieniaszko, *Intermetallics* 14 (2006) 603–606.
- [10] S.C. Tjong, Z.Y. Ma, *Mater. Sci. Eng.* R29 (2000) 49–113.
- [11] D. Tingaud, F. Nardou, *Intermetallics* 16 (2008) 732–737.
- [12] H.E. Camurla, F. Maglia, *J. Alloys Compd.* 478 (2009) 721–725.
- [13] D. Manfredi, M. Pavese, S. Biamino, P. Fino, C. Badini, *Intermetallics* 16 (2008) 580–583.
- [14] M.S. El-Eskandarany, *Mechanical Alloying for Fabrication of Advanced Engineering Materials*, Noyes Publication, Norwich, NY, 2001.
- [15] T. Mousavi, F. Karimzadeh, M.H. Abbasi, *J. Alloys Compd.* 467 (2009) 173–178.
- [16] L.Z. Zhou, J.T. Guo, G.J. Fan, *Mater. Sci. Eng. A* 249 (1998) 103–108.
- [17] K. Krivoroutchko, T. Kulik, H. Matyja, V.K. Portnoy, V.I. Fadeeva, *J. Alloys Compd.* 308 (2000) 230–236.
- [18] T.R. Smith, K.S. Vecchio, *Nanostruct. Mater.* 5 (1995) 11–23.

- [19] K.W. Ciurawa, K. Gamrat, J. Therm. Anal. Calorim. 82 (3) (2005) 719–724.
- [20] C.K. Lin, S.S. Hong, P.Y. Lee., Intermetallics 8 (2000) 1043–1048.
- [21] D. Oleszak, J. Mater. Sci. 39 (2004) 5169–5174.
- [22] S.Z. Anvari, F. Karimzadeh, M.H. Enayati, J. Alloys Compd. 477 (2009) 178–181.
- [23] V. Udhayabanu, K.R. Ravi, V. Vinod, B.S. Murty, Intermetallics 18 (2010) 353–358.
- [24] S.G. Pyo, N.J. Kim, P. Nash, Mater. Sci. Eng. 181/182A (1994) 1169–1173.
- [25] A. Albiter, M. Salazar, E. Bedolla, R.A.L. Drew, R. Perez, Mater. Sci. Eng. 347A (2003) 154–164.
- [26] O. Coreno-Alonso, J.G. Cabanas-Moreno, H.A. Calderon, F. Cruz-Gandarilla, M. Umemoto, K. Tsuchiya, International Materials Research Congress, Mexico, 2000, pp. 1–7.
- [27] J.S. Kim, S.H. Jung, Y.D. Kim, C.H. Lee, Y.S. Kwon, Mater. Sci. Forum 449–452 (2004) 1101–1104.
- [28] Y. Minamino, Y. Koizumi, N. Tsuji, et al., Sci. Tech. Adv. Mater. 5 (2004) 133–143.
- [29] T.H. De Keijser, J.I. Langford, E.J. Mittemeijer, A.B.P. Vogel, J. Appl. Crystallogr. 15 (1982) 308–314.
- [30] V. Udhayabanu, K.R. Ravi, V. Vinod, B.S. Murty, J. Alloys Compd. 497 (2010) 142–146.
- [31] D.G. Morris, X. Amils, J. Nogues, S. Surinach, M.D. Baro, M.M.A. Morris, Int. J. Non-Equilib. Process. 11 (2002) 379–409.
- [32] J. Guo, T.K.W. Huai, H.T. Li, Metall. Met. Trans. 38A (2007) 35–43.
- [33] X.H. Du, J.C. Huang, B.L. Wu, Adv. Eng. Mater. 9 (2007) 684–688.
- [34] L. Chen, Y. Han, Mater. Sci. Eng. 329–331A (2002) 725–728.
- [35] W. Chen, J.R. Hines, Y. Wang, Adv. Eng. Mater. 6 (2004) 876–879.
- [36] H. Choo, P. Nash, M. Dollar, Mater. Sci. Eng. 239A (1997) 464–471.
- [37] T. Cheng, M. McLean, Mater. Lett. 24 (1995) 377–382.
- [38] H.W. Zhang, R. Gopalan, T. Mukai, K. Hono, Scr. Mater. 53 (2005) 863–868.
- [39] K. Oh-ishi, H.W. Zhang, T. Ohkubo, K. Hono, Mater. Sci. Eng. 456A (2007) 20–27.
- [40] B. Srinivasarao, K. Oh-ishi, T. Ohkubo, K. Hono, Acta Mater. 57 (2009) 3277–3286.
- [41] P. Nash, U.C. Ur, M. Dollar, in: Proc. 2nd Int. Conf. Struct. Appl. Mech. Alloying, Vancouver, Canada, 1993, ASM International, Materials Park, OH, 192.